Supporting Information for

Coupled Plasma Etching and Electrodeposition of CoP/NiO Nanosheets with Surface Reconstruction toward Water Splitting

Qingdian Liao,[a] Tao You,[a] Xuesong Liu,[a] Kuan Deng,[a] Peng Liu,[a] Wen Tian,[a,] Junyi Ji[a, b,]**

[a] School of Chemical Engineering, Sichuan University, Chengdu 610065, P. R. China

[b] State Key Laboratory of Polymer Materials Engineering, Sichuan University, Chengdu 610065, P. R. China

* Corresponding author. E-mail address

Wen Tian, E-mail: tianwen591@scu.edu.cn

Junyi Ji, E-mail: junyiji@scu.edu.cn

Supplementary experimental section

Materials

Nickel foam (nickel purity, 99.8%); N_2 (99.9%) was purchased from Chengdu Taiyu Gas Co., Ltd. Cobalt acetate ($Co(CH_3COO)_2 \cdot 4H_2O$, AR), Nickel acetate ($Ni(CH_3COO)_2 \cdot 4H_2O$, AR), Sodium hypophosphite ($NaH_2PO_2 \cdot H_2O$, AR) and Potassium hydroxide (KOH, AR) were purchased from Shanghai Aladdin Biochemical Technology Co., Ltd; Ethanol (AR, 99.5%) and Hydrochloric acid (HCl, AR, 35-37%) were purchased from Chengdu Chron Chemicals Co,. Ltd.

Characterizations

The microstructure morphology and elemental distribution of the catalysts was characterized by scanning electron microscope equipped with energy dispersive X-ray spectroscopy (SEM, JEOL JSM-7610F) and transmission electron microscopy (TEM, JEOL JEM-F200). The crystalline structures and chemical valence states of the products were identified by X-ray diffraction (XRD, Cu Kα radiation, DX2700, Dandong Haoyuan) and X-ray photoelectron spectroscopy (XPS, PHI5000 Versa spectrometer), respectively. The Raman and ex-situ Raman was performed using DXR spectrometer (Thermal Scientific, 455 nm) and inVial (RENISHAW, 532 nm), respectively.

Electrochemical measurements

The performance in HER and OER were evaluated using a three-electrode system in 1 M KOH system (pH=14) on the electrochemical workstations (LSV, CV and i−t test was performed on CHI 760E, and EIS was performed on PARSTAT 4000A). The as-prepared composites, the Hg/HgO and graphite rod were used as working, reference and counter electrode, respectively. In order to stabilize the working electrode, all the samples were scanned by 20 cycles cyclic voltammetry (CV) at 50 mV s^{-1} before electrochemical measurements. All the potentials were referred to reversible hydrogen electrode (RHE) according to the equation[1]: $E_{RHE} = E_{Hg/HgO} + E_{RE} + 0.0592*pH$. Here, $E_{Hg/HgO}$ was the measured potentials and E_{RE} refers to the potential for the reference electrode (0.098 V for Hg/HgO electrode and 0.197 V for Ag/AgCl electrode). The linear sweep voltammetry (LSV) measurements were performed at a scan rate of 2 mV

s^{-1} and the result was collected by *iR* compensation. The LSV measurement results were fitted and calculated to obtain the Tafel slope. The equation formula of the Tafel curve is: η =a + b * log|j|. η represents the overpotential (RHE), b represents the Tafel slope and j is the current density. The EIS measurements of HER and OER were recorded at the potential of -0.100 V and 1.224 V (vs. RHE), respectively, and the frequency range is from 100 kHz to 0.01 Hz. To evaluate the C_{dl}, which was positively correlated with the electrochemical active surface area (ECSA), the CV measurements were carried out in the no-Faraday range of 0.024 V-0.124 V (vs. RHE, HER) and 1.124 V-1.224 V (vs. RHE, OER) at the scan rate of 40, 80, 120, 160 and 200 mV s^{-1}. The C_{dl} value can be estimated by plotting the current densities at different scan rates. In order to test the stability of the CoP/PNF at a large current density of 500 mA cm^{-2} in water splitting, the stability test was performed at 2.130 V (vs. RHE) without *iR* compensation for 12 h by chronoamperometry method.

Assessment of turnover frequency (TOF)

To calculate the turnover frequency (TOF), CV measurements was conducted in 1 M PBS (pH = 7) in the potential range of -0.2 ~ 0.6 V (vs. RHE) at a scan rate of 50 mV s^{-1}. Here, assuming that almost all surface active sites are accessible to the electrolyte, it is possible to evaluate TOF values in HER by the following equation[2, 3]:

$$\mathrm{TOF} = \frac{I}{2nF} \quad (1)$$

Here, I was the current (A) during the LSV measurement at a selected overpotential (0.2 V vs. RHE) in HER, F is the faraday constant (96485 C/mol), and n is the number of moles of the active sites. In this four-electron oxygen evolution reaction (2e-HER), n can be calculated by the following equation:

$$\mathrm{n} = \frac{Q}{2F} \quad (2)$$

Here, F and Q correspond to the Faraday constant (96485 C/mol) and the whole charge of CV curve (C), respectively.

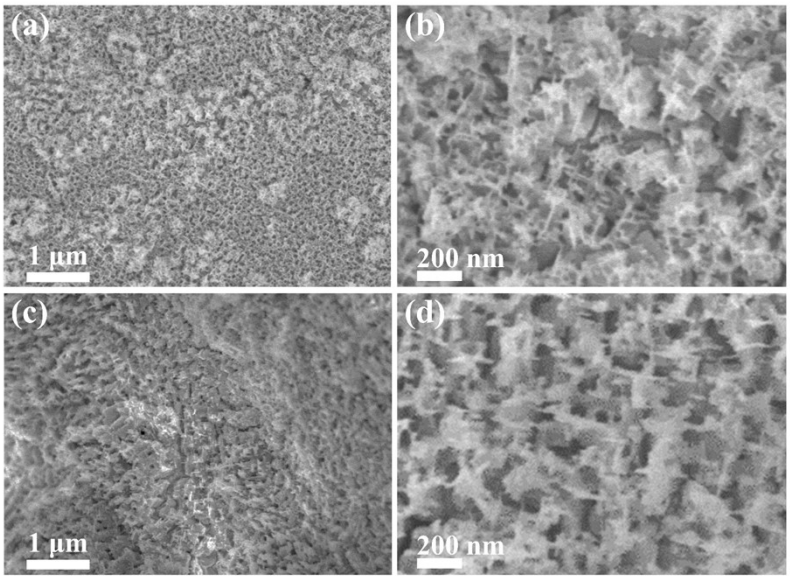

Figure S1. SEM images of the (a, b) pre-PNF and (c, d) PNF.

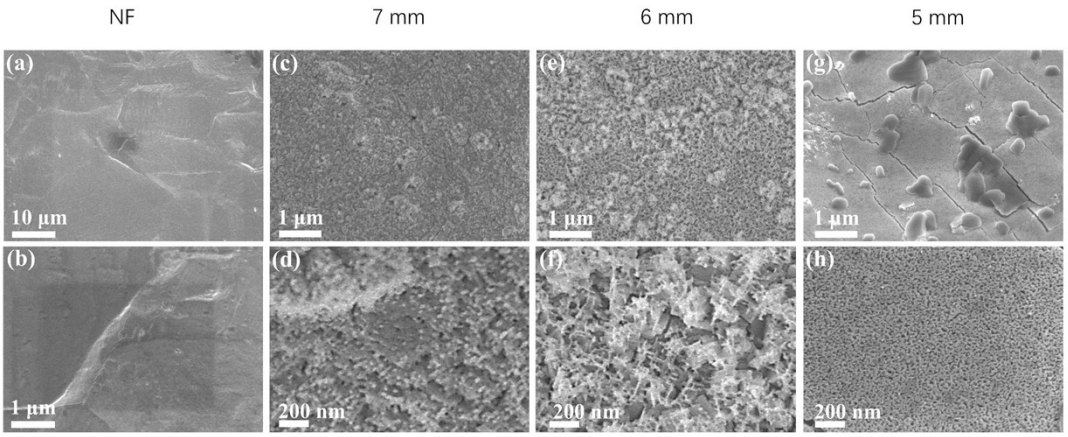

Figure S2. SEM images of the (a, b) NF and (c-h) pre-PNF with diverse etching distances spanning from 7 to 5 mm.

Figure S2 demonstrates the significant impact of different nozzle-sample distances on etching results. A small variation in distance can lead to profound changes: at 7 mm, surface etching begins, yielding sparse nanospherical structures; decreasing to 6 mm intensifies etching, resulting in dense nanoplate structures; at 5 mm, disruption of all nanoplate structures occurs, causing surface fracture, delamination, and continued etching into a porous structure, indicating a top-down etching process.

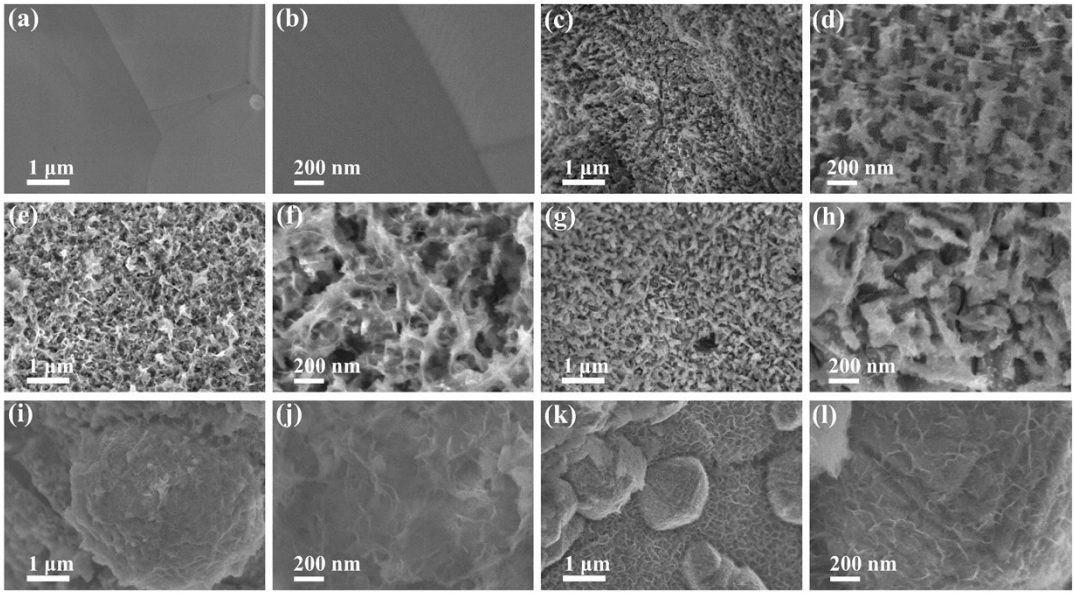

Figure S3. SEM images of (a, b) NF, (c, d) PNF, (e, f) CoP/PNF-2, (g, h) CoP/PNF-5, (i, j) CoP/PNF-10, (k, l) CoP/PNF-15.

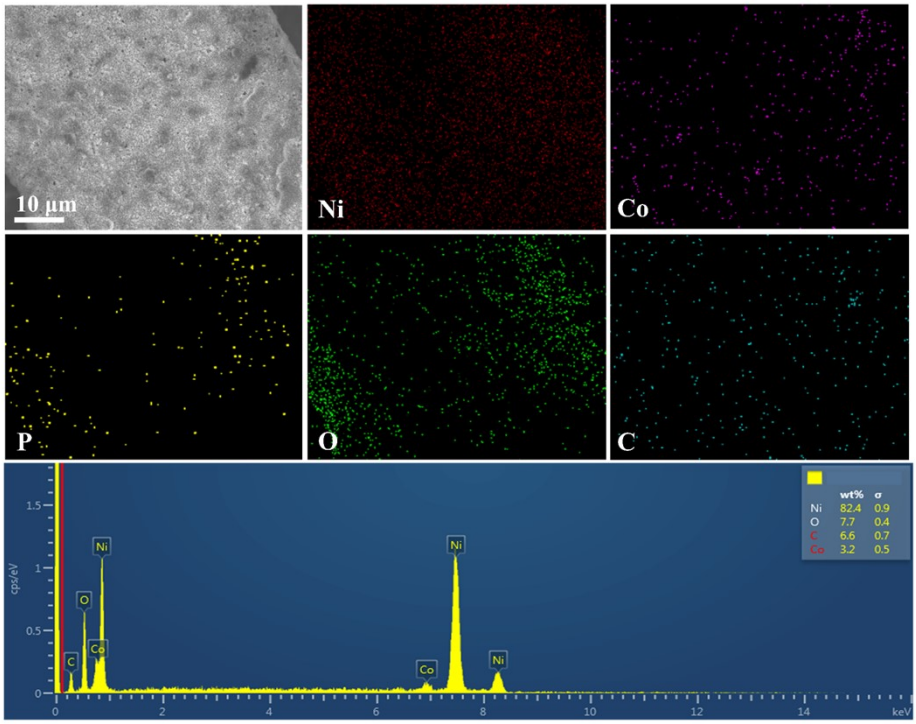

Figure S4. SEM images and the corresponding energy-dispersive X-ray spectroscopy (EDS) elemental mapping and spectra of CoP/PNF.

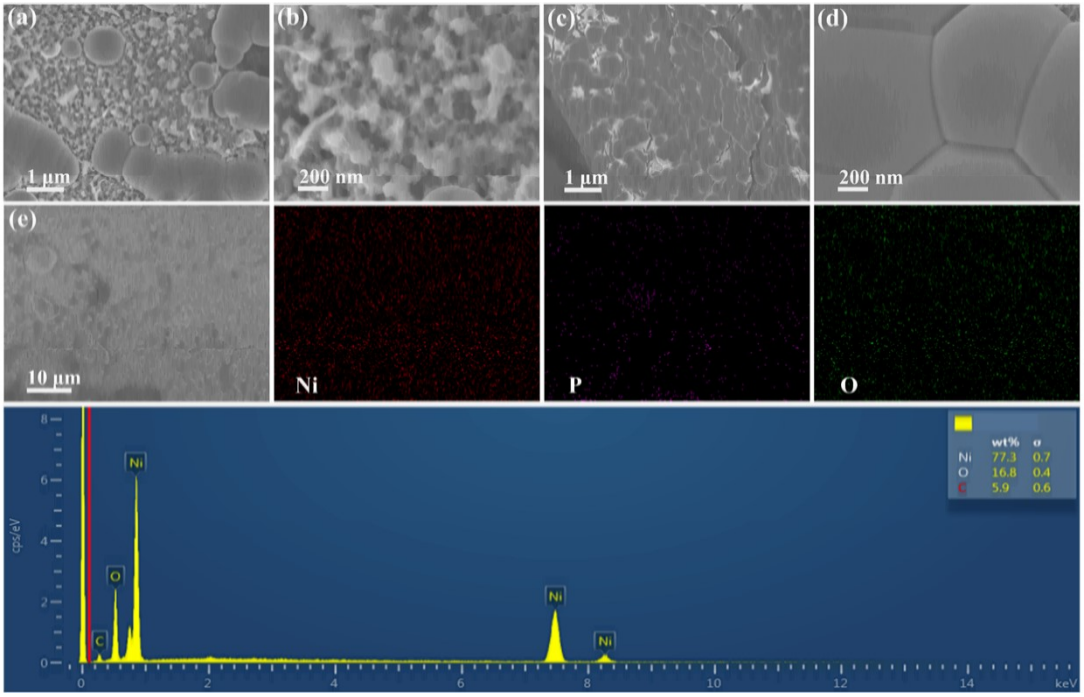

Figure S5. SEM images of (a, b) NiP/PNF-5, (c, d) NiP/PNF-10; SEM images and the corresponding energy-dispersive X-ray spectroscopy (EDS) elemental mapping and spectra of (e) NiP/PNF-5.

The characterization was conducted on the surface morphology and composition of NiP. In contrast to CoP, NiP will collect on PNF surface to generate phosphide nanospheres, which will lead to the nanosheet array being covered.

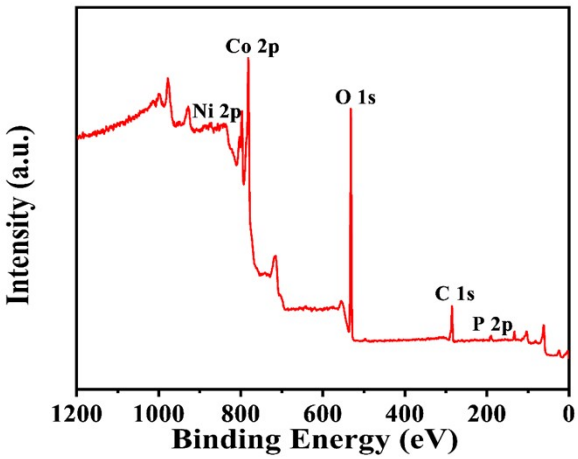

Figure S6. XPS full surveys of the CoP/PNF.

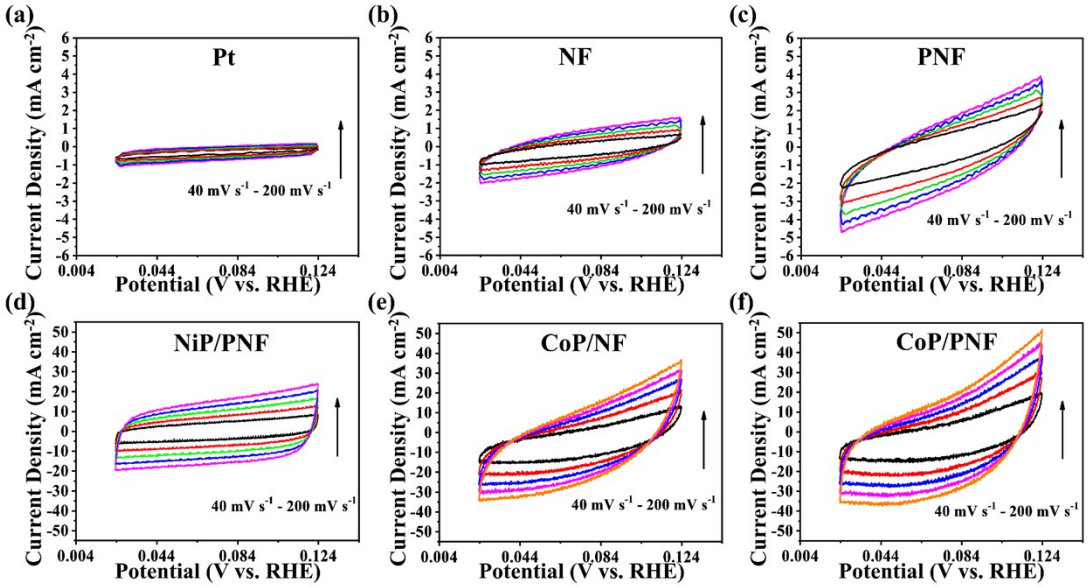

Figure S7. Cyclic voltammetry curves of the NF, PNF, NiP/PNF, CoP/NF, CoP/PNF and Pt in 1 M KOH (pH = 14) between 0.124 and 0.024 V (V vs. RHE) at different scan rate from 40 mV s^{-1} to 200 mV s^{-1}.

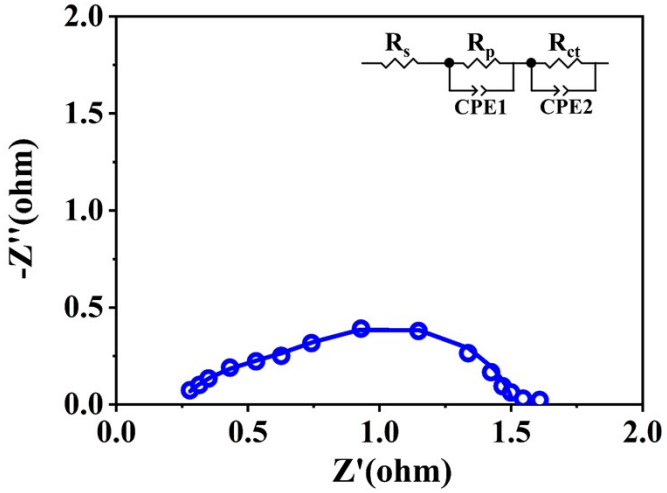

Figure S8. Nyquist plots of the Pt electrode for the HER test.

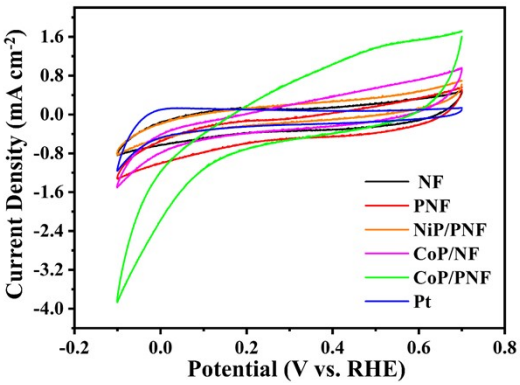

Figure S9. Cyclic voltammetry curves of the NF, PNF, CoP/PNF, NiP/PNF, and Pt in PBS buffer solution (pH = 7.4) between –0.1 V and 0.7 (V vs. RHE) at a scan rate of 50 mV s^{-1}.

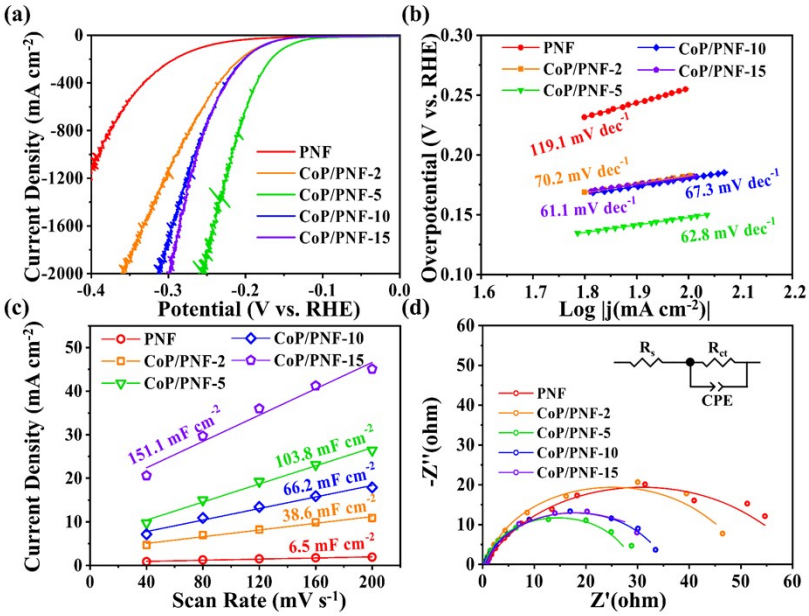

Figure S10. (a) LSV polarization curves, (b) Tafel plots, (c) estimation of C_{dl} and (d) Nyquist plots of the PNF, CoP/PNF-2, CoP/PNF-5, CoP/PNF-10, and CoP/PNF-15 in 1 M KOH during HER.

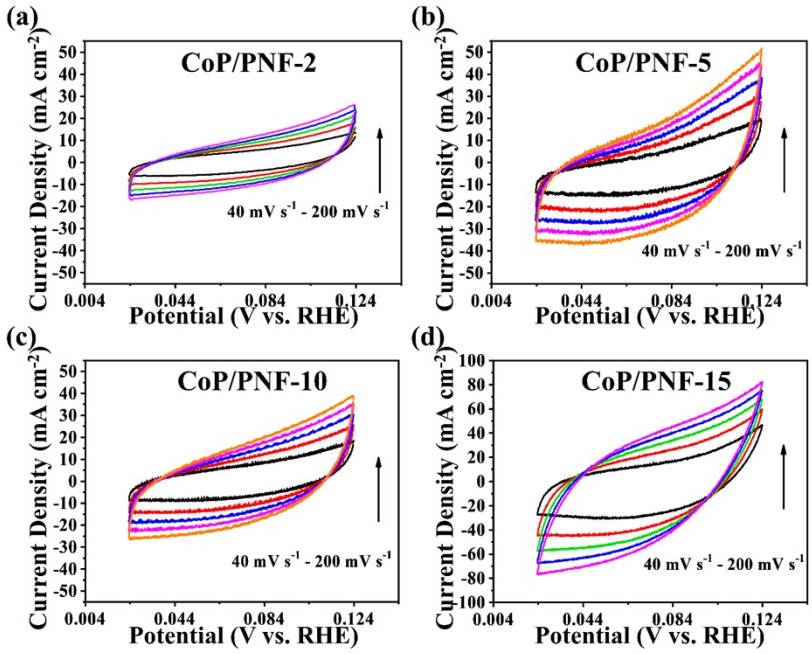

Figure S11. Cyclic voltammetry curves of the CoP/PNF-2, CoP/PNF-5, CoP/PNF-10 and CoP/PNF-15 in 1 M KOH (pH = 14) between 0.024 and 0.124 V (V vs. RHE) at different scan rate from 40 mV s^{-1} to 200 mV s^{-1}.

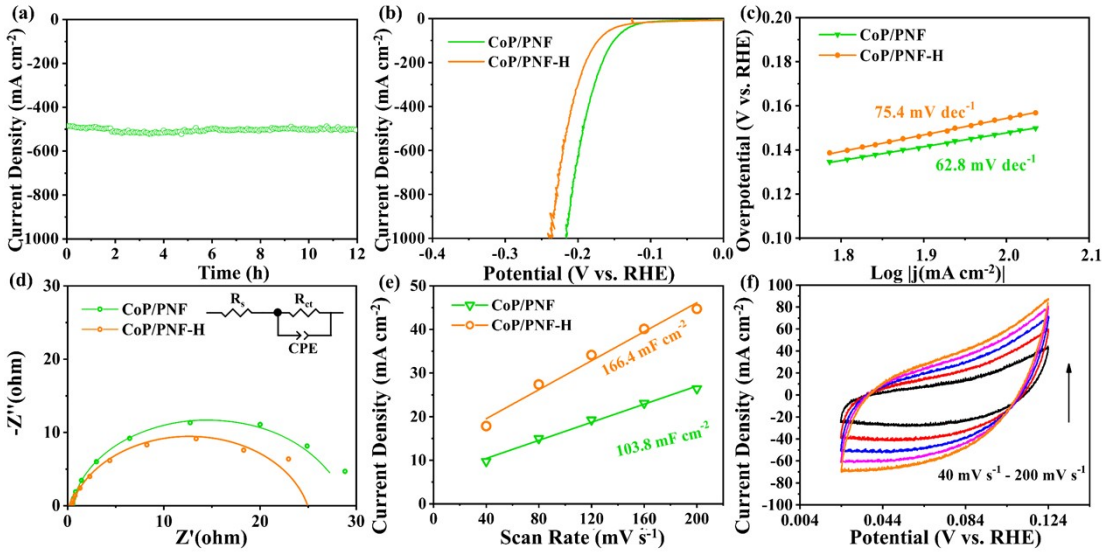

Figure S12. (a) The stability test of CoP/PNF at 500 mA cm^{-2} for 12 h HER; (b) The LSV curves, (c) Tafel plots, (d) Nyquist plots, and (e) estimation of C_{dl} for the CoP/PNF and CoP/PNF-H; (f) cyclic voltammetry curves of the CoP/PNF-H in 1 M KOH (pH = 14) between 0.024 and 0.124 V (V vs. RHE) at different scan rate from 40 mV s^{-1} to 200 mV s^{-1}.

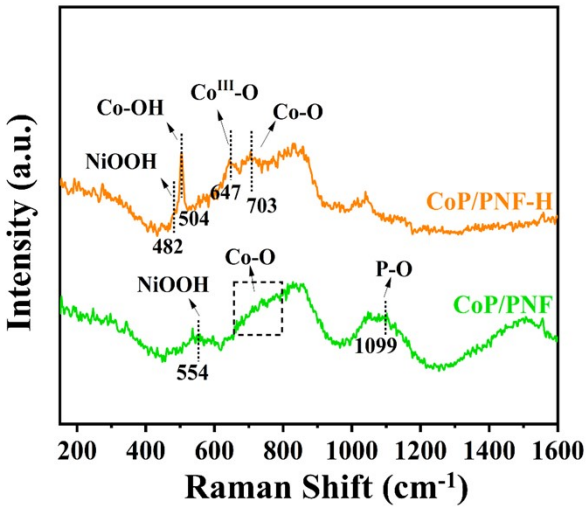

Figure S13. Raman spectra of CoP/PNF and CoP/PNF-H.

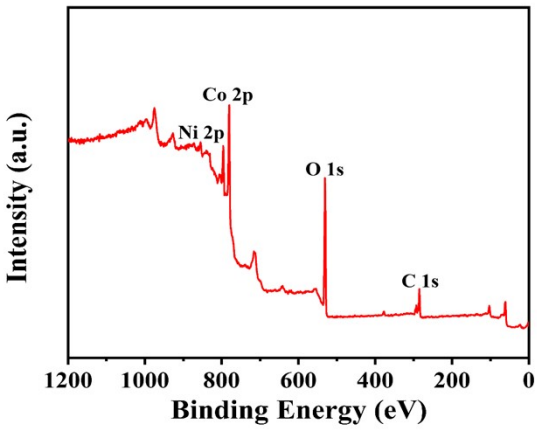

Figure S14. XPS full surveys of the CoP/PNF-H.

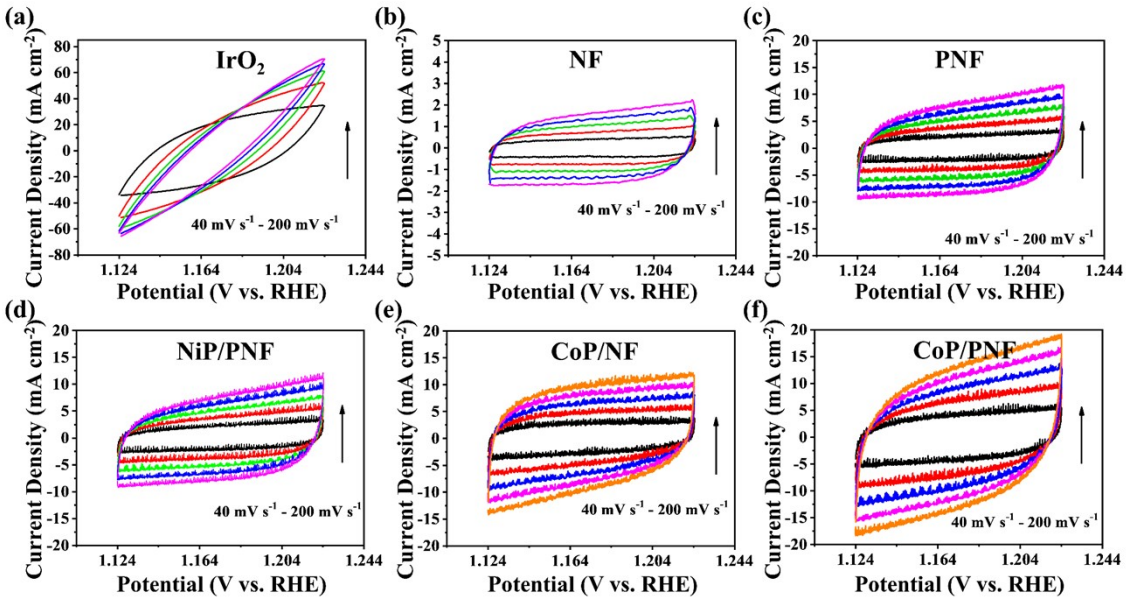

Figure S15. Cyclic voltammetry curves of the NF, PNF, CoP/NF, CoP/PNF, NiP/PNF, and IrO_2 in 1 M KOH (pH = 14) between 1.124 V and 1.224 V (V vs. RHE) at different scan rate from 40 mV s^{-1} to 200 mV s^{-1}.

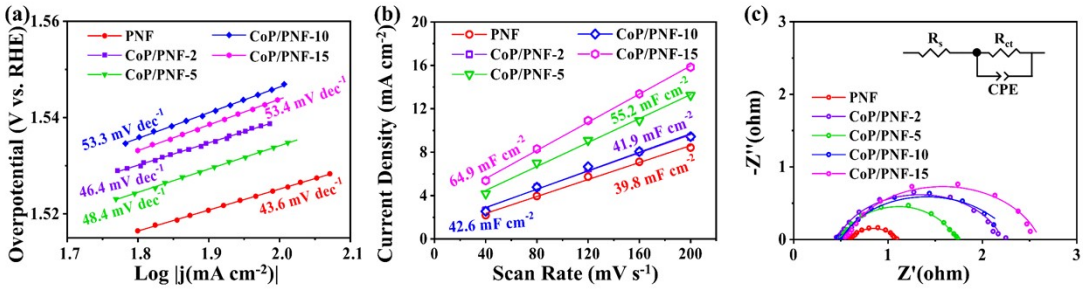

Figure S16. (a) Tafel plots, (b) estimation of C_{dl} and (c) Nyquist plots of the PNF, CoP/PNF-2, CoP/PNF-5, CoP/PNF-10, and CoP/PNF-15 in 1 M KOH during OER.

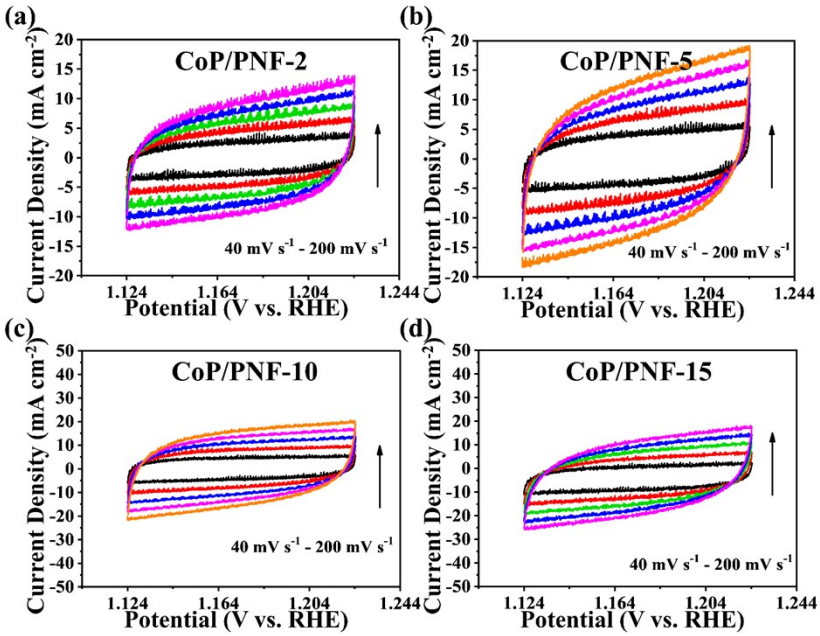

Figure S17. Cyclic voltammetry curves of the CoP/PNF-2, CoP/PNF-5, CoP/PNF-10 and CoP/PNF-15 in 1 M KOH (pH = 14) between 1.124 V and 1.224 V (V vs. RHE) at different scan rate from 40 mV s^{-1} to 200 mV s^{-1}.

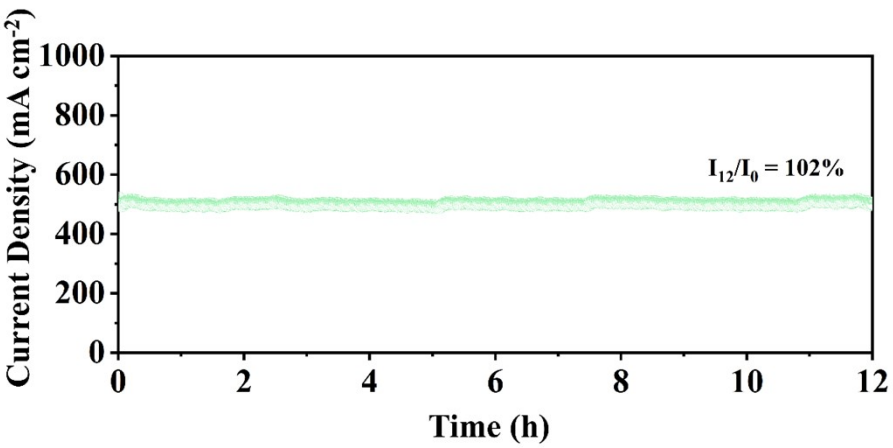

Figure S18. The stability test of CoP/PNF at 500 mA cm^{-2} for 12 h OER.

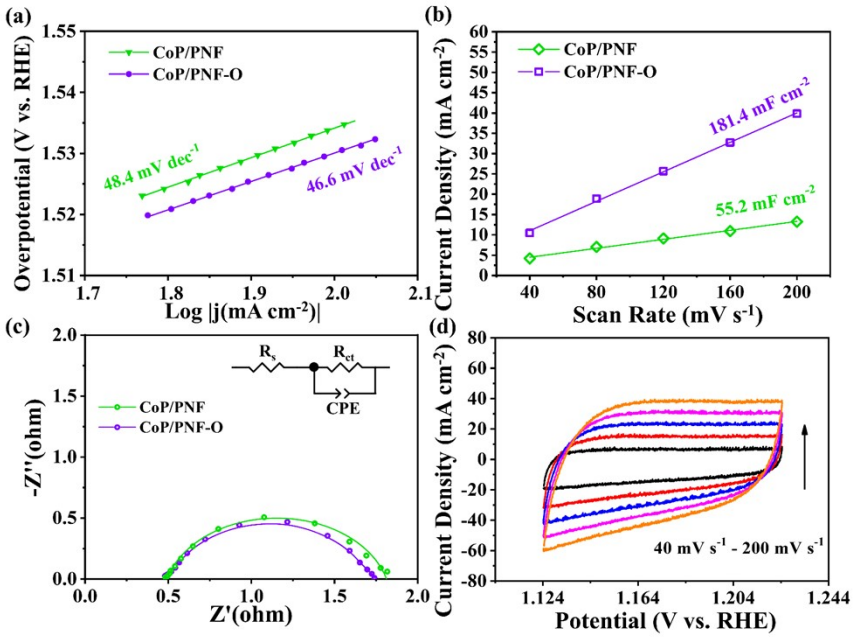

Figure S19. (a) Tafel plots, (b) estimation of C_{dl}, and (c) Nyquist plots for the CoP/PNF and CoP/PNF-O; (d) cyclic voltammetry curves of the CoP/PNF-H in 1M KOH (pH = 14) between 1.024 and 1.124 V (V vs. RHE) at different scan rate from 40 mV s^{-1} to 200 mV s^{-1}.

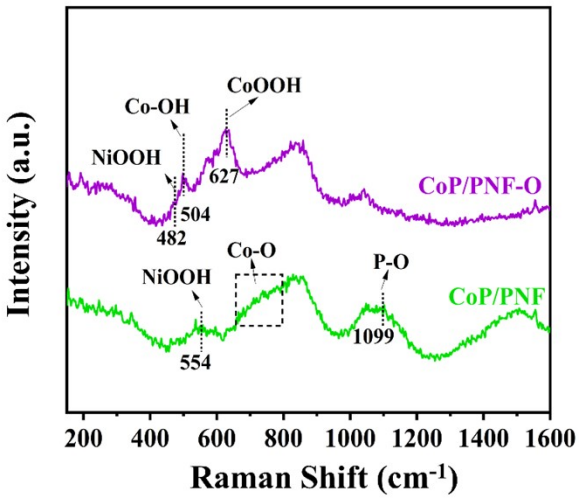

Figure S20. Raman spectra of CoP/PNF and CoP/PNF-O.

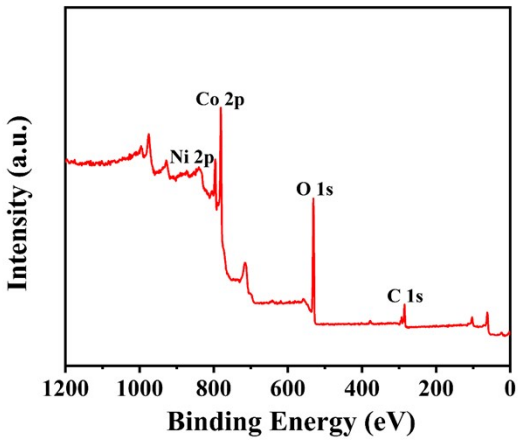

Figure S21. XPS survey spectrum of CoP/PNF-O.

Table S1. The elemental composition of CoP/PNF, CoP/PNF-H and CoP/PNF-O determined by XPS.

Samples	Co (%)	Ni (%)	P (%)	O (%)	C (%)
CoP/PNF	19.22	1.11	4.19	51.68	23.79
CoP/PNF-H	16.23	2.60	0	53.69	27.48
CoP/PNF-O	20.23	1.14	1.43	52.40	24.69

Table S2. The ratio of M^{3+}/M^{2+} in CoP/PNF, CoP/PNF-H and CoP/PNF-O determined by XPS.

Samples	the ratio of M^{3+}/M^{2+}	
	Co^{3+}/Co^{2+}	Ni^{3+}/Ni^{2+}
CoP/PNF	0	0.71
CoP/PNF-H	2.12	0.54
CoP/PNF-O	1.07	1.06

Table S3. Fitting values of Nyquist curves of various composite for HER.

Electrode material	R_s (Ω)	R_{ct} (Ω)	CPE2-T	CPE2-P	R_p (Ω)	CPE1-T	CPE1-P
NF	0.7535	76.1700	0.0011	0.8113	-	-	-
PNF	0.6184	60.5300	0.0025	0.7422	-	-	-
NiP/PNF-5	0.6006	45.9500	0.0040	0.8462	-	-	-
CoP/NF	0.7688	37.2300	0.0162	0.8496	-	-	-
CoP/PNF-2	0.7083	48.8400	0.0061	0.8843	-	-	-
CoP/PNF-5	0.5004	28.0900	0.0144	0.9187	-	-	-
CoP/PNF-10	0.5478	34.3500	0.0119	0.8491	-	-	-
CoP/PNF-15	0.6710	34.4444	0.0288	0.8485	-	-	-
Pt	0.2354	0.7662	0.0046	0.9144	0.5074	0.0042	0.6922

Table S4. The correlation between the CV deposition count of CoP and the mass loading.

Electrode material	Mass loading (mg cm^{-2})
CoP/PNF-2	0.19
CoP/PNF-5	0.65
CoP/PNF-10	2.31
CoP/PNF-15	4.31

Table S5. Fitting values of Nyquist curves of various composite for OER.

Electrode material	R_s (Ω)	R_{ct} (Ω)	CPE-T	CPE-P
NF	0.7994	34.2000	0.0061	0.7889
PNF	0.5986	0.4963	0.0931	0.7182
NiP/PNF	0.7178	1.4310	0.0468	0.8106
CoP/NF	0.7402	9.1610	0.0170	0.8251
CoP/PNF-2	0.4570	1.7330	0.0468	0.8101
CoP/PNF-5	0.5082	1.2220	0.0465	0.8314
CoP/PNF-10	0.5270	1.7350	0.0424	0.7909
CoP/PNF-15	0.5574	2.0500	0.0531	0.8138
IrO_2	1.1850	0.6428	0.3385	0.7958

Table S6. comparison of the voltages required to reach 10 mA cm^{-2} with the reported high-end cells.

Electrode materials	Substrates	η_{10} (V)	Referenc
CoP/PNF||CoP/PNF	Ni foam	1.545	This work
IrO_2/Ti||Pt	-	1.575	This work
$Fe_{1.2}(CoNi)_{1.8}Se_6$ MESe||$Fe_{1.2}(CoNi)_{1.8}Se_6$ MESe	-	1.550	[4]
F–Fe–CoP NS|| F–Fe–CoP NS	Ni foam	1.570	[5]
$Co(OH)_2/Fe_7Se_8$||$Co(OH)_2/Fe_7Se_8$	-	1.620	[6]
$(Fe_{0.27}Ni_{0.35}Co_{0.24}Cr_{0.10}Mn_{0.04})_2O_{3-\delta}$ HEOs||HEOs	-	1.550	[7]
Pt/C||Co-1T-MoS_2/C	Carbon	1.570	[8]
Mo–NiCoP@MXene/NF||Mo–NiCoP@MXene/NF	Ni foam	1.560	[9]
$Fe_{0.4}Co_{0.3}Ni_{0.3}$-1.8||$Fe_{0.4}Co_{0.3}Ni_{0.3}$-1.8	-	1.620	[10]
FeOOH/S-Co/NF||FeOOH/S-Co/NF	Ni foam	1.576	[11]
CNFMPO||CNFMPO	Ni foam	1.540	[12]
N-$NiMoO_4$/Ni/CNTs||N-$NiMoO_4$/Ni/CNTs	-	1.640	[13]
Cu_3P/Ni_2P@CF||Cu_3P/Ni_2P@CF	Carbon	1.560	[14]
MoNiFe||MoNiFe	Ni foam	1.550	[15]

References

1. T. Xu, D. Jiao, M. Liu, L. Zhang, X. Fan, L. Zheng, W. Zheng and X. Cui, *Advanced science (Weinh)*, 2023, **10**, e2205605.
2. K. T. Le, N. N. T. Pham, Y.-S. Liao, A. Ranjan, H.-Y. Lin, P.-H. Chen, H. Nguyen, M. Y. Lu, S. G. Lee and J. M. Wu, *Journal of Materials Chemistry A*, 2023, **11**, 3481-3492.
3. X. Liu, P. Liu, F. Wang, X. Lv, T. Yang, W. Tian, C. Wang, S. Tan and J. Ji, *ACS Applied Materials & Interfaces*, 2021, **13**, 41545-41554.
4. H. Wu, Z. Wang, Z. Li, Y. Ma, F. Ding, F. Li, H. Bian, Q. Zhai, Y. Ren, Y. Shi, Y. Yang, Y. Deng, S. Tang and X. Meng, *Advanced Energy Materials*, 2023, **13**, 2300837.
5. D. Xu, S. Liu, M. Zhang, L. Xu, H. Gao and J. Yao, *Small*, 2023, **19**, e2300201.
6. C. Gong, L. Zhao, D. Li, X. He, H. Chen, X. Du, D. Wang, W. Fang, X. Zeng and W. Li, *Chemical Engineering Journal*, 2023, **466**, 143124.
7. S. Liao, T. Huang, W. Wu, T. Yang, Q. Hou, S. Sang, K. Liu, Y. Yang and H. Liu, *Chemical Engineering Journal*, 2023, **471**, 144506.
8. K. Nie, N. Li, B. Li, Y. Yuan, Y. Zhang, P. Liu, S. Chong, J. Hu, Z. Liu and W. Huang, *Chemical Engineering Journal*, 2023, **475**, 146066.
9. J. Jiang, R. Sun, X. Huang, W. Xu, S. Zhou, Y. Wei, S. Han and Y. Li, *Composites Part B: Engineering*, 2023, **263**, 110834.
10. Y. Chen, L. Yang, C. Li, Y. Wu, X. Lv, H. Wang and J. e. Qu, *Energy & Environmental Materials*, 2023, **0**, e12590.
11. Z. Zang, Y. Ren, X. Li, Y. Cheng, L. Li, X. Yu, X. Yang, Z. Lu, X. Zhang and H. Liu, *Journal of Materials Chemistry A*, 2023, DOI: 10.1039/d3ta05613a.
12. H.-M. Zhang, L. Zuo, Y. Gao, J. Guo, C. Zhu, J. Xu and J. Sun, *Journal of Materials Science & Technology*, 2024, **173**, 1-10.
13. G. L. Li, X. Y. Qiao, Y. Y. Miao, T. Y. Wang and F. Deng, *Small*, 2023, **19**, e2207196.
14. H. Liu, J. Gao, X. Xu, Q. Jia, L. Yang, S. Wang and D. Cao, *Chemical Engineering Journal*, 2022, **448**, 137706.
15. N. S. Gultom, T.-S. Chen, M. Z. Silitonga and D.-H. Kuo, *Applied Catalysis B: Environmental*, 2023, **322**, 122103.